Drag Reduction of Natural Laminar Flow Airfoils with a Flexible Surface Deturbulator

Sumon.K.Sinha[*]
Sinhatech
3607 Lyles Drive, Oxford, MS.

Sundeep Vijay Ravande [†]
Mechanical Engineering Dept.
University of Mississippi

A flexible composite surface deturbulator (FCSD) has been developed in order to stabilize large extents of thin separated flow over aerodynamic surfaces through passive interactions with a streamwise varying pressure gradient boundary layer flow. This accelerates the external flow since skin friction is mitigated, while attenuating turbulent dissipation in the separated region. In this study this effect has been used to reduce drag and increase lift of natural laminar flow airfoils at low Mach numbers with Reynolds numbers ranging from 3×10^5, which is typical of long endurance unmanned aerial vehicles, to 6×10^6 typical of many general aviation aircraft. Wing profile drag reduction of 10-20% was observed in high-Re flight tests with a NLF-0414F wing. Low-Re wind tunnel measurements on the NLF-0414F have shown a profile drag reduction of 60-80% including a 45% reduction in pressure drag, along with a 12% increase in section lift coefficient. This doubled the L/D from 12.5 to 25.7. A full-span upper surface FCSD treatment of an earlier generation Wortmann FX-S-02196 natural laminar flow wing indicated a 5-20% increase in total aircraft L/D over the range of flyable airspeeds.

Nomenclature

A	=	wing area
AFW	=	active flexible wall transducer
C_d	=	drag coefficient ($D / (qA)$)
C_p	=	pressure coefficient (($p_{static} - p_{static,\infty}$) $/ q$)
C_l	=	lift coefficient ($L / (qA)$)
c	=	chord length
D	=	drag force
s	=	center to center distance between two strips
FCSD	=	flexible composite surface Deturbulator
f	=	flow-FCS interaction frequency
L	=	lift force on airfoil
M	=	Mach number
$p_{static,\infty}$	=	upstream static pressure

[*] *President,* Sinhatech, Oxford, MS, Senior Member AIAA and Associate Professor of Mechanical Engineering, University of Mississippi

[†] *Student Member,* AIAA and Graduate Student, University of Mississippi.

$p_{stag,\infty}$	=	upstream stagnation pressure
q	=	up stream dynamic pressure ($\rho\, U^2_\infty\, /2$)
Re	=	Reynolds number based on the chord length of the airfoil ($\rho\, U_\infty\, c\, /\, \mu$)
St	=	Strouhal number ($f\,d\, /\, U$)
U	=	local free stream velocity
U_∞	=	upstream velocity
u	=	fluid velocity in the stream wise direction
v	=	fluid velocity normal to the stream wise direction
x	=	distance from the leading edge along the chord;
	=	coordinate along the stream wise direction
y	=	coordinate normal to the unexcited flexible wall
α	=	angle of attack
δ	=	hydrodynamic boundary layer thickness
δ_1	=	boundary layer displacement thickness
δ_2	=	boundary layer momentum thickness
μ	=	dynamic viscosity
v	=	kinematic viscosity of the fluid
ρ	=	density
NLF	=	Natural Laminar Flow

I.   Introduction

In 2005 crude oil prices rose 50% to their highest level since the invasion of Kuwait and thet have continued to increase in 2006. The "International Energy Agency" has forecast a 60% rise in global gas demand and 50% for oil by 2010. The ever increasing demand with increasing fuel prices is going to become a catastrophe to the airline industry. US airlines claim that they paid USD 6 billion more for fuel in 2005 compared to 2004. Reduction of fuel consumption by aircraft can be achieved by reducing drag and enhancing lift. This is beneficial for all aircraft, ranging from large commercial transports to unmanned aerial vehicles and sailplanes. Aircraft designers optimize the general aerodynamic configuration, including wing sizes and shapes, in order to obtain the lowest possible drag during cruise.   In order to improve aerodynamic efficiency NASA developed the Natural Laminar Flow (NLF) airfoil series in 1970's based on computer optimization techniques[1]. The aim was to increase L/D of general aviation aircraft (business jets and sport aviation). Profiles were optimized to maintain laminar flow up to X/C = 0.5c, while making sure that premature transition did not degrade performance below comparable non NLF airfoils even when manufacturing imperfections and roughness buildup due to leading edge bug hits and surface deicing also were taken into account.

Sailplane designers, as well as designers of high altitude long endurance UAV's have pursued the NLF philosophy more aggressively, since wing surface roughness has been minimized by extensive use of composite materials. Only recently composite materials and reduced surface roughness they offer are beginning to make headway in the commercial aviation market. Super critical airfoils used by subsonic jet transport aircraft also have their maximum thickness points as far aft as possible similar to NLF wings, even though their form is to limit drag buildup due to the onset of shock induced boundary layer separation under transonic conditions. Surface pressures on both NLF and supercritical airfoils typically remain nearly constant over a significant region across the chord. The profile of the aft pressure recovery region of the airfoil is dictated primarily by a desire to limit boundary layer separation. The ideal profile in this respect is the Stratford zero-wall-shear. However, this implies keeping the boundary layer on the verge of separation. This is nearly impossible to maintain over a range of wing loading, airspeeds and altitudes. Any additional drag reduction requires manipulating the airflow to alter the fundamental drag generation mechanisms.

While NLF or Laminar Flow Control (LFC) has traditionally been employed to reduce drag for subsonic airfoils, the availability of new materials and fabrication techniques has opened up new vistas in drag reduction through boundary layer flow control. One such method that has shown promise is the Flexible Composite Surface Deturbulator (FCSD) shown in Figs 1a-c. The FCSD is a micro-structured compliant wall[2], and interaction of compliant walls with zero-pressure gradient laminar, transitional and turbulent boundary layers is well documented[3,4]. The uniqueness of the FCSD approach is that it relies on reducing the overall aerodynamic drag by helping maintain a thin layer of separated flow near the surface by attenuating turbulent mixing in this shear layer[5]. The presence of a varying chord-wise pressure gradient, typical of airfoils and streamlined aerodynamic bodies is essential for this. The FCSD helps maintain a laminar separation bubble-like flow structure, except that it is stretched over a larger extent of the chord. In this manner the bubble behaves as a slip-layer to the external flow and can eliminate skin-friction drag. Laminar boundary layers have
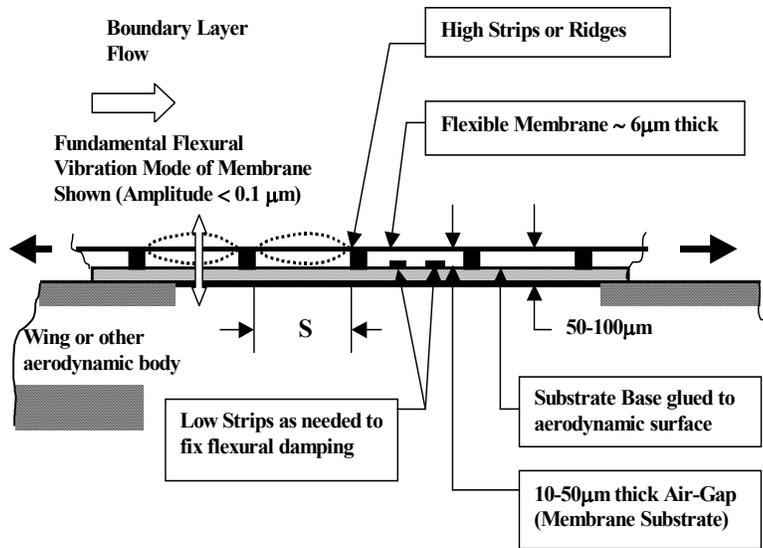
American Institute of Aeronautics and Astronautics

Fig 1a. Schematic of the SINHA Flexible Composite Surface (FCSD)

lower skin-friction compared to turbulent boundary layers. However unlike the FCSD approach, promotion of laminar flow alone cannot zero out skin friction. In practice, FCSD modification of boundary layer flows significantly lowers skin friction coefficients as evidenced by a speed up of the external inviscid flow. This can help increase circulation and lift generation similar to Liebeck high-lift airfoils[6]. Such airfoils, however require close control of transition. The FCSD makes transition control less critical, thereby extending the low drag conditions to larger ranges of flight conditions. Also, earlier compliant wall research was done for mainly for water flows since, the mechanical properties of compliant surfaces responsive to air flows would make them extremely delicate and hence impractical[4]. The FCSD has overcome this limitation by its unique construction technique, interaction mechanism and integration with the wing.

This paper focuses on flow modifications resulting from integrating the FCSD with existing low-drag airfoils which rely on maintaining laminar flow over an extended region of the chord.

Fig 1b. Photograph of FCSD strip on wing showing effect on near surface flow visualized with oil (Flow is from left to right)

**The Flexible Composite Surface Deturbulator** (SINHA-FCSD, Fig 1a), is currently prototyped by Sinhatech (www.sinhatech.com) in the form of a 50-100-μm thick, 10-60 mm wide micro-flexural tape (Fig 1-b). The complete installation on aircraft wings requires surface mounted flow pre-conditioners to enhance the interaction of the FCSD with the boundary layer airflow. The SINHA-FCSD is the subject of applications for U.S. and International Patents (PCT) by Sinha (2003a)[2]. It is an improvement over the previously patented (Sinha, 1999) electrically actuated Active Flexible Wall (AFW) transducer[7]. When affixed to an appropriate location, the constrained-mode flexural oscillations of the FCSD membrane couples dynamically with boundary layer and free-stream turbulent fluctuations and force the fluctuations to move to the high-frequency dissipation range[8]. This causes a dramatic reduction in turbulence levels, which is further exploited for reducing drag as described below.

II.   Theoretical Understanding

Much of the direct interaction of the AFW or FCS is within a few microns from the surface of the membrane and cannot be directly measured, experimentally visualized, or computationally modeled in a simple manner. Compared to oscillatory blowing and synthetic jets, which require actuation jet velocities around the same order of magnitude as the freestream velocity (Washburn et al., 2002)[9], typical membrane velocities of the AFW or FCS are four orders of magnitude lower (under 3-mm/s for a 50 m/s boundary layer freestream velocity). Also the interaction frequency is much higher and scales with the unsupported free length (s in Fig 1) of the membrane instead of larger length scales, such as the distance of the actuator from the wing or flap trailing edge. Hence, there is no question that the interaction mechanism is different. Unlike earlier compliant and driven flexible wall devices which were typically tested on flat-

Free stream
$\partial U/\partial t \approx v(\partial u/\partial y)_{y=0}$

Flow of pressure fluctuations

$\partial p/\partial x < 0$

$\partial p/\partial x \cong 0$

$\partial p/\partial x > 0$

SINHA-FCS
(Membrane Oscillation velocity v)

Separation point

Separated Shear Layer
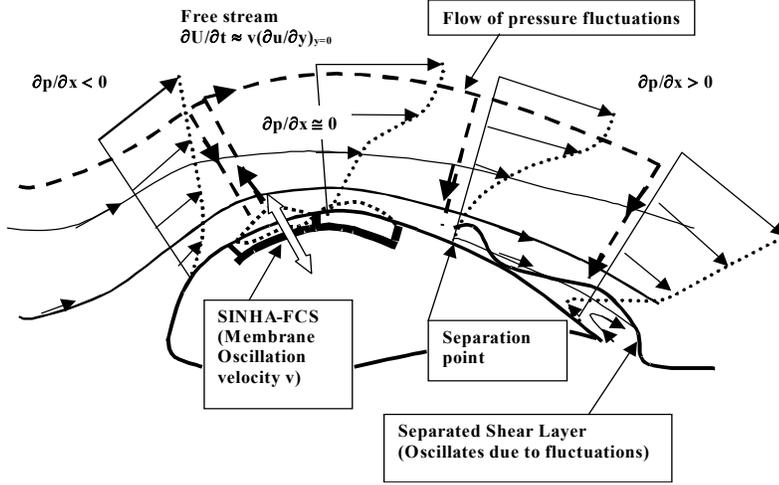(Oscillates due to fluctuations)

Fig 1c. Schematic of the interaction of the SINHA-Flexible Composite Surface with a streamwise varying pressure gradient boundary layer on an airfoil. Thickness exaggerated for clarity.

plate zero pressure gradient flow (Bushnell and Heffner, 1987)[3], the AFW has been found to work only in boundary flows exposed to a streamwise varying pressure gradient as shown in Fig 1c. To understand the flow-membrane interaction mechanism the 2-D streamwise u-momentum equation of the flow at the mean equilibrium position (y = 0) of the surface membrane of the FCS is considered first:

$$v(\partial u/\partial y)_{y=0} = -(1/\rho)(\partial p/\partial x) + (\mu/\rho)(\partial^2 u/\partial y^2)_{y=0} \qquad (1)$$

The streamwise x-component of velocity "u" of the vibrating membrane (or the velocity of the fluid at the points of contact with the membrane) has been assumed to be negligible, while the wall-normal y-component of velocity "v" of the fluid next to the membrane is clearly non-zero due to membrane compliance. Key to flow-membrane interaction is the realization that the wall-normal gradient of the streamwise velocity at the wall, $(\partial u/\partial y)_{y=0}$, can be extremely large at certain x-locations. At such locations, even a small oscillation velocity (v << U) of the flexible membrane can make the $v(\partial u/\partial y)_{y=0}$ "control" term on the left hand side of equation (1) predominant. For a non-porous, non-compliant wall, this control term is identically zero. Additionally, if the boundary layer velocity profile at the aforementioned locations is such that prior to interaction $\partial^2 u/\partial y^2_{y=0} \approx 0$, while $|(\partial u/\partial y)_{y=0}| > 0$, (i.e., u(y) is approximately linear near the wall) an order of magnitude balance of the terms in equation (1) yields:

$$v(\partial u/\partial y)_{y=0} \approx -(1/\rho)(\partial p/\partial x) \qquad (1-a)$$

Such a condition can be satisfied in boundary layers over curved surfaces, in the vicinity of x-locations where the streamwise pressure gradient $\partial p/\partial x$ changes from favorable ($\partial p/\partial x < 0$) to adverse ($\partial p/\partial x > 0$), as shown in Fig 1c. What makes such locations unique is the large relative change in $\partial p/\partial x$ introduced through equation (1-a), since $\partial p/\partial x \approx 0$ prior to this interaction. The interaction will however make the initially linear velocity profile u(y) nonlinear. This will also contribute towards viscous dissipation, which will be in addition to dissipation due to the internal damping of the FCS.

For boundary layer flows, pressure variation across the boundary layer ($\partial p/\partial y$) is negligible, and the streamwise pressure gradient $\partial p/\partial x$ can be obtained from the inviscid momentum equation at the outer, or freestream edge of the boundary layer:

$$(\partial U/\partial t) + U (\partial U/\partial x) = -(1/\rho) (\partial p/\partial x) \qquad (2)$$

For x-locations where equation (1-a) holds, an oscillatory motion of the wall can, therefore, directly introduce fluctuations in the freestream velocity U, through the pressure gradient term. For example, in a steady boundary layer flow over a rigid non-porous wall, the pressure gradient term on the right hand side of equation (2) will be completely balanced by the non-linear convective term on the left hand side. If this flow is perturbed, by introducing a small wall-normal velocity v through flexible wall motion, the resulting fluctuations in the pressure gradient will have to be balanced by the unsteady term (∂U/∂t) in equation (2). For x-locations where ∂p/∂x $\approx$ 0 in the un-modified flow, as required for ensuring the validity of equation (1-a), the overall effect of wall motion can be expressed as:

$$\partial U/\partial t \approx v(\partial u/\partial y)_{y=0} \qquad \qquad (3)$$

Streamwise u-velocities will be perturbed at the wall oscillation frequency in this manner throughout the thickness of the boundary layer. The fluctuations will however, maximize at the outer edge due to the absence of viscous terms, as verified experimentally (Sinha, 2001)

It is important to note that equation (3) holds irrespective of the source of the perturbations. The discussions thus far have presumed the source to be the flexible wall. However, equation (3) also describes how fluctuations in the freesteam velocity U can impart oscillations to a compliant wall at x-locations where equation (1-a) remains valid (Sinha and Zou, 2000)[10]. If fluctuations exist in the freestream velocity U, as is normally the case in most external aerodynamic flows, the presence of a compliant wall around the ∂p/∂x $\approx$ 0 location results in partitioning the energy of the fluctuations between the fluid and the wall (Carpenter et al, 2001)[4]. The degree of partitioning at any instant depends on the temporal phase of the wall oscillation cycle.

The vibratory response of the wall also plays a key role in this interaction. The predominant response of the SINHA FCS can be expected to be flexural. The maximum displacements and energy storage capacity of the FCS corresponds to the fundamental mode as per the sketch of the deflected membrane in Figs 1c. Dissipation can also be expected to be higher for higher modes of flexural oscillation, especially if the low strips constrict the airflow across them. As a mass of disturbed freestream fluid approaches a segment of the SINHA FCS membrane, where equation (1-a) holds, the membrane begins to undergo flexural displacement. The membrane continues to deflect as the disturbed fluid convects over it. At some point the displaced membrane begins to swing back, initiating the reverse phase of the oscillation cycle. In the process of deflecting to its extreme position, the membrane and substrate of the FCS store a significant portion of the flow fluctuation kinetic energy as elastic potential energy. As the membrane springs back, most of this energy is released back to the flow. However, the original fluid particles, which had provided this energy, would have convected downstream by a distance U.Δt during the time interval Δt taken by the membrane to execute one oscillation cycle. For the re-released energy to be imparted to the same mass of fluid that originated it, the following condition must hold:

$$\mathbf{U.\Delta t = s} \qquad \qquad (4)$$

where, s = the free length of the membrane of the SINHA FCS, between two ridges.

This condition imposes the membrane oscillation frequency: f = U/s, and is a manifestation of "traveling wave flutter" (Carpenter et al, 2001)[4].

The aforementioned process results in sustaining fluctuations corresponding to f, while attenuating fluctuations at other frequencies. The efficacy of the selection process depends on the ability of the FCS to damp out higher modes, while minimizing damping in the fundamental flexural mode corresponding to f. Also, the spacing s has to be sufficiently close such that equations (1-a) and (3) hold throughout this region. The frequency selection criterion and the conditions needed for small amplitude wall motion to influence the freestream also hold for the

active flexible wall transducer and have been validated in all experiments run to date[11,12].
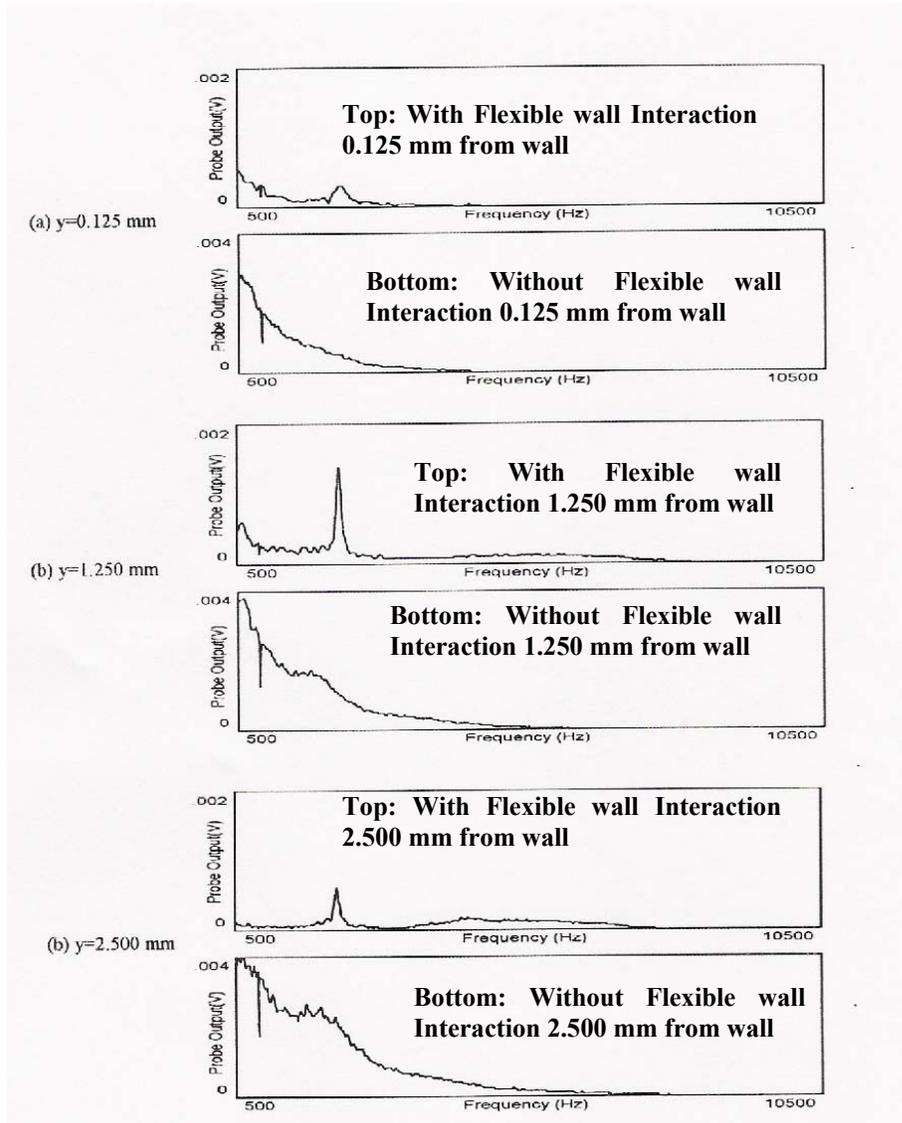

Fig 1d. Experimental evidence of modification of boundary layer velocity spectra due to flexible wall interaction. Hot-wire probe output (Volts) versus frequency (Hz) is for separated airflow 90° from stagnation over a 152-mm diameter cylinder at Re = 0.15M at three separate distances (y-positions) from the wall from Sinha and Wang, 1999[8].

Fig 1c shows experimental evidence of the interaction frequency (f = 2.25 kHz in this case) in a boundary layer flow over a cylinder, slightly downstream of separation[8]. The data were obtained with the AFW transducer incorporating a pre-tensioned membrane having flexural natural frequencies significantly different from f. "With Flexible wall Interaction" implies electrically driving a section of the AFW at frequency f. Without interaction is without the aforementioned electrical actuation. The frequency spectrum clearly shows the inability of the flow to support fluctuations at frequencies other than f. Even though the un-actuated AFW is the FCSD, the high pre-tension in the membrane attenuates flow-induced membrane oscillation. However, such interaction still exists as evidenced from the broad-band peak in the vicinity of f in the "Without Flexible wall Interaction" velocity spectrum farthest from the wall at y = 2.500 mm. This is a direct manifestation of Equation (3).

III.   Experimental Setup

The NLF-0414F airfoil developed by NASA Langley was selected as the test airfoil since an all composite single engine trainer, the Global GT-3[11] was available for testing which incorporated this airfoil. However, at low Re values typical of long-endurance UAVs the ability to improve L/D values for this airfoil was also important. Hence, a low speed wind-tunnel was used for the low-Re tests with flight tests on the GT-3 for the higher-Re investigations.

Low-Re Wind Tunnel Measurements

NLF-0414F wind-tunnel wing model: A 127-mm (5-inch) chord electro-discharge wire-cut aluminum airfoil was custom made as shown in Fig 3. All tests were carried out in the slow speed windtunnel having a test section 9-inches wide, 12-inches high, 14-inches long as shown in Fig 2. The surface of the model was polished with 1000 grit emory paper. The 7.75-inch (197-mm) span wing model was supported in between two Plexiglas end plates in order to constrain the corner vortices. The flow in the middle 100-mm span of the wing model was used for tests with measurements being conducted in the central vertical plane. All tests were run at the maximum speed setting of the tunnel (Re = 0.3M, M = 0.09) with the airfoil at an angle of attack α set at -1°. The value of α was based on the design cruise angle of attack of the wing mid-span of the GT-3 trainer (Sinha, 2001) which incorporates the NLF-0414F airfoil.

Figure 2: Sinhatech Slow-speed Wind-Tunnel   **Figure 3: Close up of tunnel section showing the NLF-0414F airfoil**

Instrumentation: A 5-μm diameter miniature hot-wire (HW) probe with a 1-channel Mini-CTA constant temperature anemometer from Dantec Corp. was used to measure boundary layer velocities and turbulence levels. The HW probe was calibrated before and after test runs against a system of 1.58 mm diameter static and total head probes placed within 6-mm from the HW in the wind tunnel. A micrometer traverse with a least count of 20-μm was used to position the probe. Temperature-compensated electronic differential pressure transducers, calibrated against a Dwyer inclined tube manometer, were used to measure pressures. Pressure measurements were also used in wake total pressure averaging drag rakes spanning a region of 41-mm (Fig 4). The difference in total pressures between the upstream and wake can be used to estimate the C_d resulting from each surface as shown below[5,13]. Drag rake measurements were used in the wind tunnel as well as in flight tests to screen the efficacy of the FCSD installations. A reduction in the drag rake pressure difference characterized by $C_{pDR} = \Delta P_{DR} /(\rho U_\infty^2/2)$ indicates drag reduction and vice versa. A pair of similar drag rakes mounted on the upper and lower surfaces of the flap trailing edge was used in the flight tests of the GT-3 aircraft outlined below. Due to a difference in the static pressures on the upper and lower surfaces, the upper and lower rakes were connected individually to two separate pressure transducers in the flight tests. A separate 127-mm long drag rake was used at about 50% chord behind the wind-tunnel model in order to determine the total profile drag in the final tests.

In-Flight Drag reduction and Boundary layer measurements

Flight Test Setup: Flight tests were conducted on the all-composite single-engine 3-passenger (including pilot) trainer aircraft with a NLF-0414F. The aircraft was operated from the premises of ATI at the Starkville airport. An on board 40-channel pressure scanner employing individually calibrated differential silicon pressure transducers, along with a laptop computer based data acquisition system was used. For wing boundary layer

velocity profile measurements the high-pressure sides of the pressure transducers were connected to the individual tubes of the boundary layer mouse (BLM)[18]. The low-pressure sides were connected to the static-pressure tube of the BLM. For drag tests two drag-rakes (Fig 4) arranged above and below the trailing edge of the flap were connected to the low-pressure sides of two of the transducers. The high-pressure sides were connected to a wing-bottom mounted total head probe spaced far enough apart to pick up the upstream stagnation pressure. In this arrangement a leak in the drag rake causes the transducers to read high (i.e., drag increase). Hence any reduction in the transducer outputs truly represents a drag reduction.

In any given flight either the two drag rakes (DR) or the BLM mounted at a given position could be used. Furthermore, the BLM could not be used upstream of or on top of the FCSD. Typically, the aircraft was topped with fuel every three or four flights lasting about 25-35 minutes. The pilot took the aircraft to the test altitude (typically around 200 ft pressure altitude) and held a constant airspeed ranging from 95-109 knots indicated airspeed (KIAS) while a second person in the passenger seat operated the laptop-based data acquisition system to acquire voltages from the pressure transducers. The data acquisition system scanned through the entire set of transducers at 100-kHz, averaged 100 readings per transducer and stored the raw voltages for further processing into pressures and velocities.

IV.   Results

Initial tests on the NLF-0414F wing of the GT-3 (Sinha 2001) showed the FCSD capable of speeding up the boundary layer flow on the bottom of the wing. Furthermore, the ability of the FCSD in reducing drag in spite of leading edge boundary layer tripping was also demonstrated. In this study the effect of FCSD flow control at both low (Re = 0.3 M) and high Reynolds numbers (Re = 6-M) and low subsonic Mach numbers (M < 0.2) is investigated.

Figures 6 and 9 show pressure distributions on a NLF-0414F airfoil predicted with the XFOIL 6.94[14]. All simulations were carried out for angles of attacks varying from 2 to -2 degrees for Reynolds number of 300000 and 6000000 respectively. Fig 7 shows the measured pressure distributions on the wind tunnel wing model. An integration of measured static pressures was used to compute lift and pressure drag coefficients. The FCSD is seen to increase the section C_L from 0.244 to 0.273 (or 12%), while reducing the section pressure-drag coefficient C_{DP} from 0.019 to 0.010 (or 45%). This boosts the C_L/ C_{DP} from **12.5 to 25.7**. Drag rake measurements, with the 127-mm wake mounted rake, indicated a reduction in stagnation pressure drop (C_{pDR}) of 52%. This also indicates that the FCSD reduced both pressure-drag and skin-friction-drag. The ratio of C_{DP}/ C_D for this low-Re (Re = 311,000) case is about 4/5 for the clean wing as indicated by the XFOIL simulation. This is approximately the same as the ratio of reduction the two drag coefficients (i.e., $\Delta C_{DP}/ \Delta C_D$).

The locations of 5-mm wide FCSD strips on both the upper and lower surfaces of the NLF-0414F wind tunnel model are proprietary. They are based on the criteria depicted in equations (1) with some modifications to account for the separated flow near the trailing edge at these low Reynolds numbers. The lower surface FCSD had significant sections of the membrane glued to the substrate, reducing its efficacy. The upper FCSD was free of this defect. Hence the lower-surface FCSD impeded the flow. At the same time reduction in viscous losses on the upper surface helped accelerate the suction-surface flow, thereby increasing lift. Determining the optimum FCSD positions required a number of trials. Fig 8 shows boundary layer velocity profile measurements for an earlier (FCSD-2) treatment and compares it to the clean wing. The profiles clearly show de-turbulation as a reduction in rms velocity fluctuations. The boundary layer velocity profile integral analyses yielded that the FCSD reduced the displacement thickness from 0.99-mm (clean wing) to 0.65-mm and reduced the momentum thickness from 0.35-mm to 0.23 mm, increasing the kinematic shape factor from **2.82 to 2.87.**

GT-3 Aircraft Drag Reduction Estimates: Installing 50-mm wide, 600-mm long FCSD panels, with the FCSD substrate leading edges at suitable (currently held proprietary) X/C locations   produced 2-9% increase in boundary layer momentum at 78% of the chord on the lower surface and virtually no change on the upper surface. Even though these locations were the same as the earlier AFW/FCSD installations (Sinha 2003), the current adhesive backed substrate was thinner than the earlier etched substrate when mounted with double-sided adhesive tape. Instead of thickening the substrate, which can increase flow blockage, optimizing the chordwise location of the FCSD based on the actual measured pressure distributions was selected. An additional factor influencing this decision was the large increase in skin friction on the upper surface of the flap and at the higher Reynolds numbers as evidenced in XFOIL simulations of the NLF-0414F airfoil. Figure 10 shows the

contribution of the upper and lower surfaces towards total wing profile drag over the range of indicated airspeeds tested along with change in total drag due to non-optimal FCSD treatments. Figures (11a–11d) show boundary layer velocity profiles at 90%-chord on the upper surface throughout the cruise speed range.
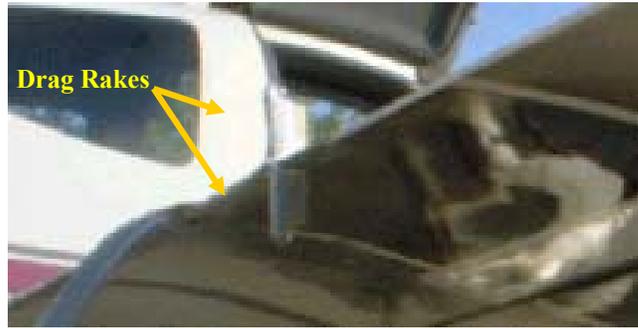

Figure 4: Drag rakes mounted on the trailing edge of the GT-3 wing

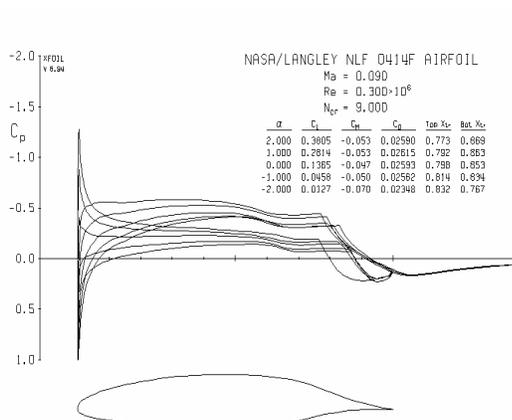**Figure 5: GT-3 showing the pressure transducer array on top of the wing**

Fig 6: Pressure Distribution over a NLF-0414F wing for various for various AOA varying from 2 degrees to – 2 degrees @ Re 300000 (XFOIL 6.94)

and momentum thickness at 0.90c is shown in figure 12.

Figure 12 show the drag reductions resulting from the aforementioned treatment calculated. The maximum drag reduction of about 20% occurred at the best cruising speed of 105-KIAS with a minimum reduction of 11% at the lowest speed tested. The relative contribution of each surface treatment towards the reduction in overall section C_D at each Re were based on the clean-wing trends shown in Figure 10. The displacement

American Institute of Aeronautics and Astronautics

The locations of FCSD strips for this case (proprietary) were significantly different compared to the low-Re wind tunnel model. This is not surprising considering the difference in flow separation characteristics between the two cases (Figs 6 and 9). It was also unclear if the reduction in profile drag at the higher flight Reynolds numbers was accompanied by lift increase seen at lower Re (Fig 7).
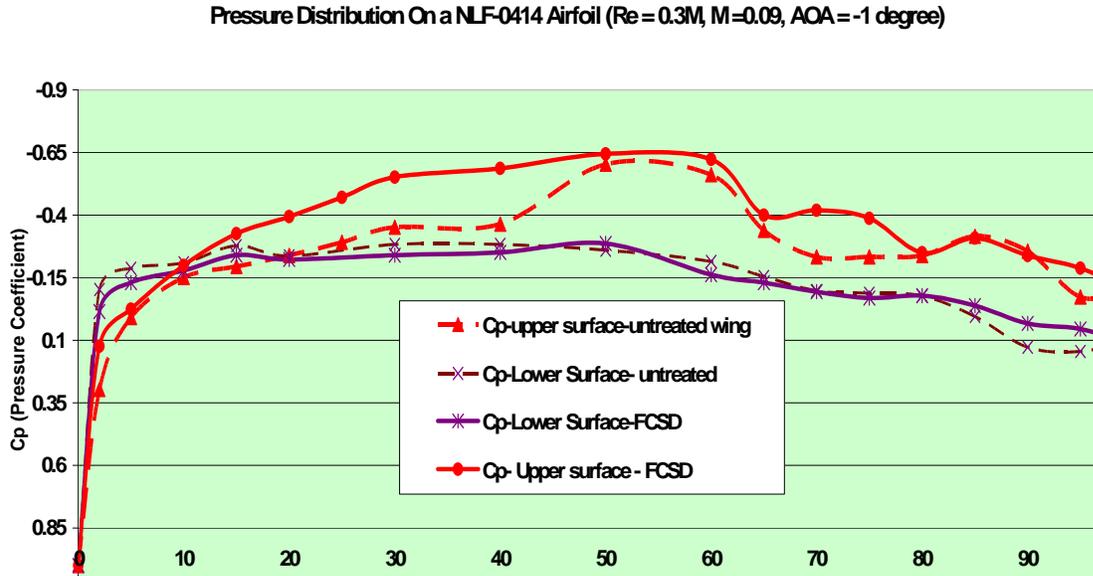
Pressure Distribution On a NLF-0414 Airfoil (Re = 0.3M, M=0.09, AOA = -1 degree)

Fig 7: Pressure Distribution on NLF-0414F airfoil model tested in the SINHATECH wind-tunnel showing the effect of FCSD flow control at low Reynolds numbers
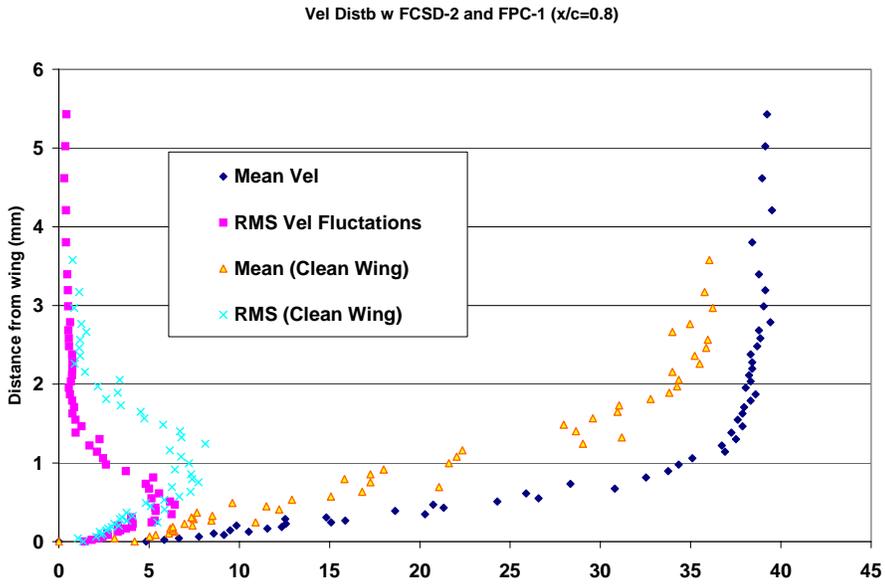
Fig 8. Boundary Layer Velocity Profiles at x/c = 0.8 on top surface of NLF-0414F wind tunnel model (Re = 0.3M, α = -1º, M =0.09) with and without FCSD-2
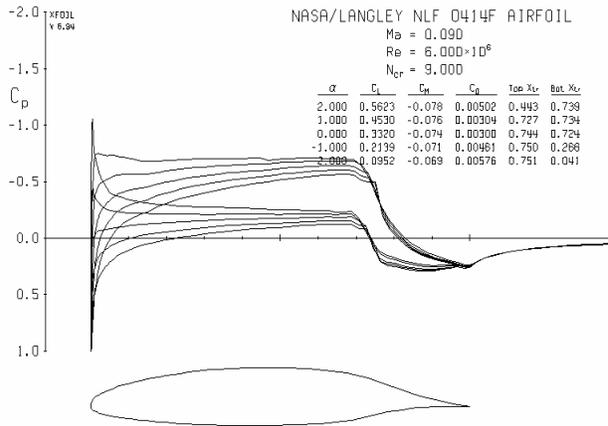
Fig 9: Pressure Distribution over a NLF-0414F wing for various for various AOA varying from 2 degrees to – 2 degrees @ Re 6-million (XFOIL 6.94)
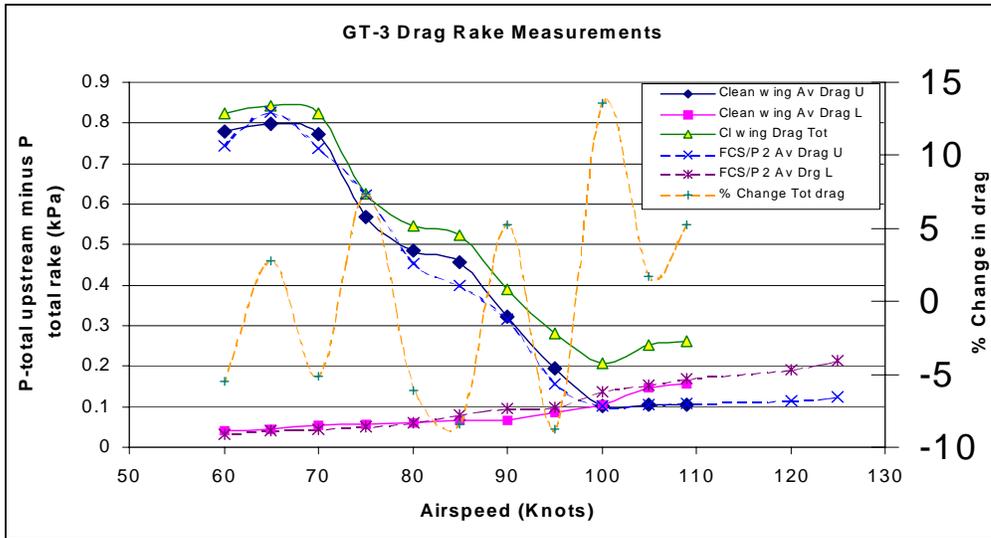
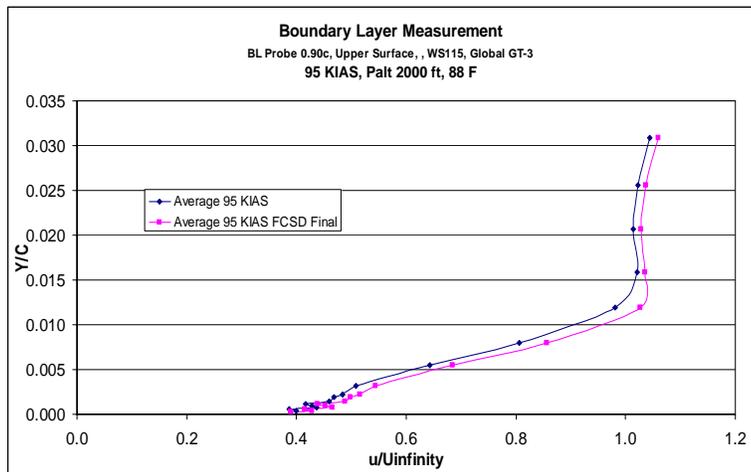**Fig 10. Profile drag contributions from upper and lower surfaces on GT-3 wing**

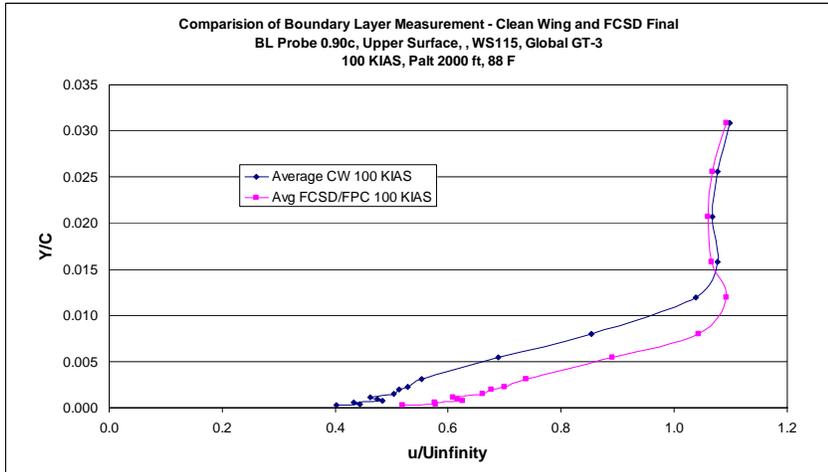**Fig 11a: Suction surface boundary layer velocity profiles at 95 KIAS on a GT-3 Aircraft wing at 0.90c**
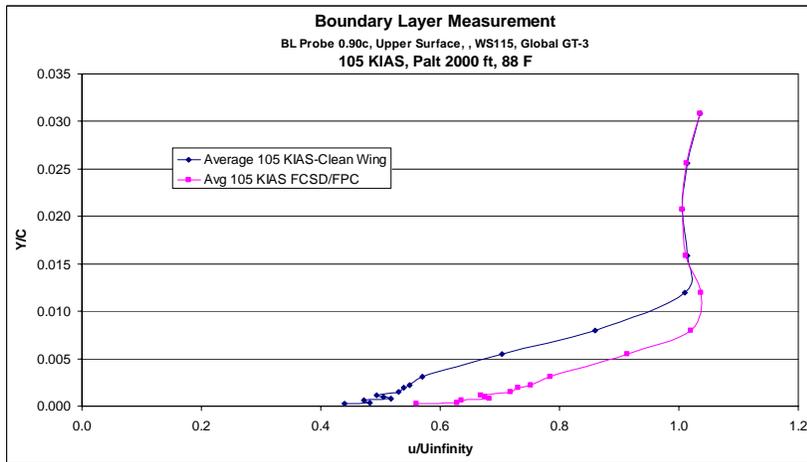
American Institute of Aeronautics and Astronautics

Fig 11b: Suction surface boundary layer velocity profiles at 100 KIAS on a GT-3 Aircraft wing at 0.90c

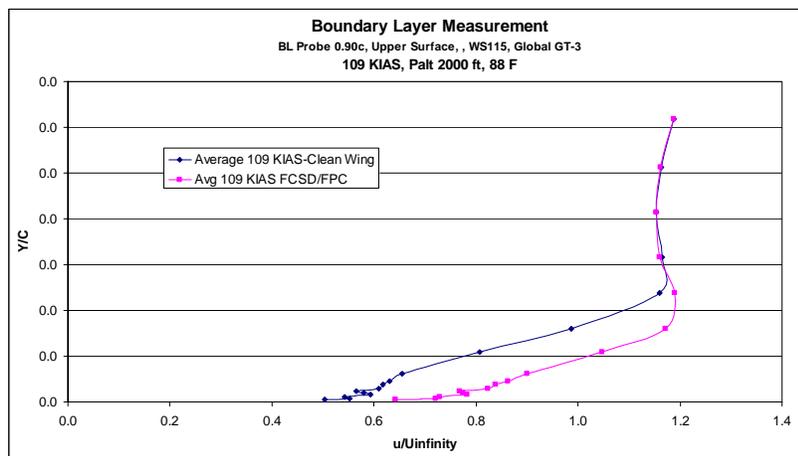**Fig 11c: Suction surface boundary layer velocity profiles at 105 KIAS on a GT-3 Aircraft wing at 0.90c**

Fig 11d: Suction surface boundary layer velocity profiles at 109 KIAS on a GT-3 Aircraft wing at 0.90c

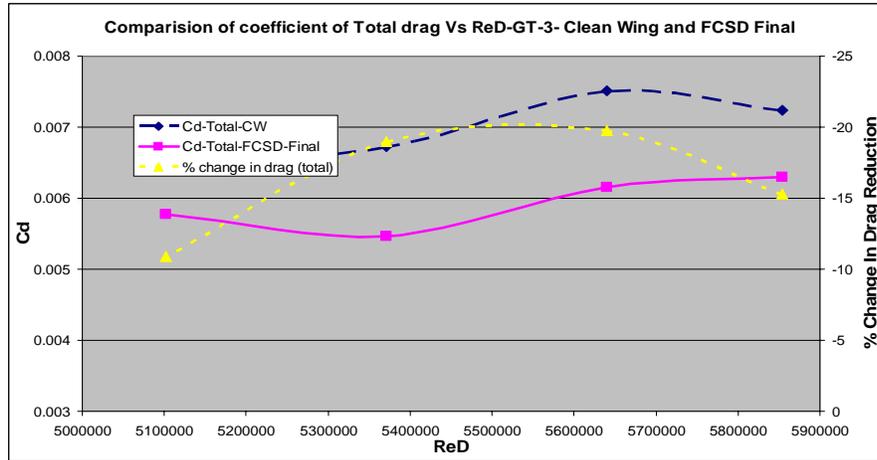American Institute of Aeronautics and Astronautics

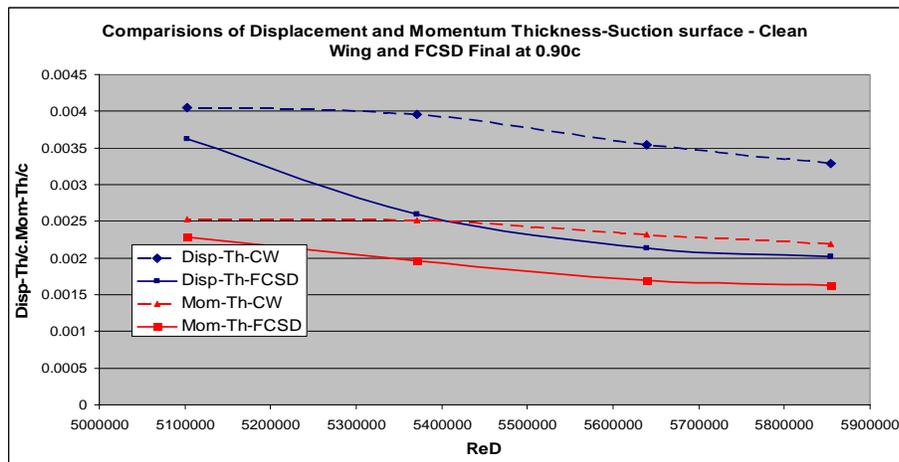**Fig 12: Comparison of total drag Vs Re – Clean wing and wing with FCSD**

Fig 13: Comparison of Displacement thickness and momentum thickness at 0.90c on the suction surface of a GT-3 Wing

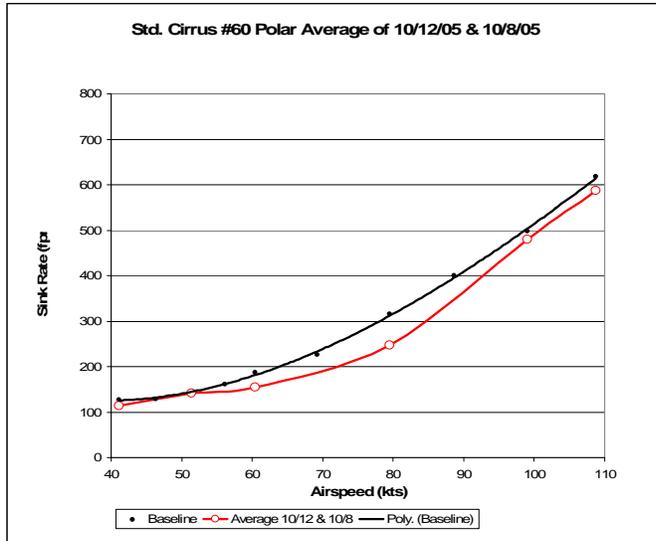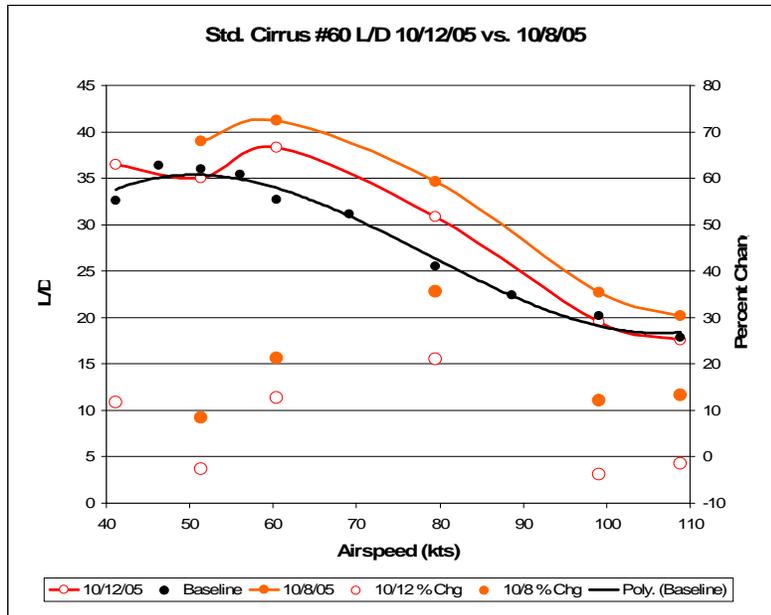American Institute of Aeronautics and Astronautics

Fig 14. In-Flight Sink-Rate (top) and L/D measurements (bottom) of a Standard Cirrus Sailplane with Wortmann "natural laminar flow" airfoils, with (red) and without (black) full-span upper-surface FCSD treatment

Flight Performance Tests on a Wortmann earlier generation Natural Laminar Flow Airfoil:

In order to determine the effect of FCSD treatment on aircraft performance, flight sink rate measurements were conducted on a Standard Cirrus sailplane with fiberglass composite wings incorporating variations of the older generation Wortmann FX-S-02196 natural laminar flow airfoil[5,13]. Surface oil flow revealed transition on the upper surface of the wing around 55% of the chord. Earlier wind tunnel tests of selected wing section airfoils revealed L/D improvement of 400% at a Reynolds number of about 300,000. Unlike the NLF-0414F, the flow separation and transition characteristics of the Wortmann airfoils remained unaffected over the range of Reynolds numbers studied (0.3 million to 3 million). Fig 14 shows the reduction in sink rate and improvement in L/D ratios over the flyable airspeed range as a result of full-span top surface FCSD treatment. The best L/D increases from about 36 to 40, but occurs at a higher airspeed. Movements of the atmospheric air mass cause the parallel shift in the two L/D curves. The more conservative data of 10/12/05 is believed to be closely approximate the true behavior, which shows a 20% enhancement in L/D at 80-kts. We are in the process of obtaining more data on different days to obtain a truly representative average.

American Institute of Aeronautics and Astronautics

V.   Conclusions

A passive flow control device has been developed that can be affixed to selected X/C locations on natural laminar flow wing surfaces to reduce wing profile drag as well as the induced drag. Induced drag is expected to reduce if a wing section generates more lift compared to the untreated case at a given airspeed. Wind tunnel tests have shown that the FCSD creates a virtual wing profile with a thin region (under 1μm) of dead air along with low turbulence levels all through the chord. The FCSD mitigates the profile drag by stabilizing the near wall shear layer (Fig 15.).

All Wind-tunnel and in-flight boundary layer measurements have clearly indicated a fuller profile (i.e. similar to a turbulent boundary layer) with a thin region of marginally separated flow indicated in some oil flow tests. Though the flow is slightly separated over a significant portion of the chord and classical fluid dynamics would have suggested an increase in drag with such a flow structure, our measurements show decrease in drag. This is achieved by reducing the turbulence levels as mentioned earlier using the FCSD in such a flow structure. This reduces the skin friction (C_f) and speeds up the flow on the upper surface, yielding lower coefficient of pressure (C_p) and higher lift.

At low-Re for the NLF-0414F airfoil, total profile drag and section pressure drag are reduced in spite of a significant separated zone remaining in the wake. The only explanation for this is that lower turbulence levels in the wake convert the wake into a virtual boat tail extension. This opens up the possibility of using the FCSD to reduce form drag on bluff or un-streamlined objects. Recent wind tunnel tests have validated this possibility (Sinha and Sinha, 2007).

The drag reduction mechanism and the drag reduction data has been clearly outlined in this investigation on two different aircraft built with different airfoils. The extended span treatment on a sail plane[20] has shown an increase in the L/D (at Re 3000000) of existing sailplanes by retrofitting the existing wings. The results thus obtained create an opportunity to retrofit all subsonic fixed wing aircraft to reduce drag thus making them more fuel efficient.

The optimized FCSD has the potential of reducing overall fuel consumption of large transport aircraft by at least 10% through retrofitting, resulting in similar reductions in fossil fuel usage and emissions of NO_x and greenhouse gases. . The enhancement of lift measurements obtained could make the complicated flap structure on a commercial aircraft simpler, thereby reducing the weight and drag of the aircraft. This along with reducing the profile drag and induced drag using the FCSD tape could make the existing aircrafts highly fuel efficient.
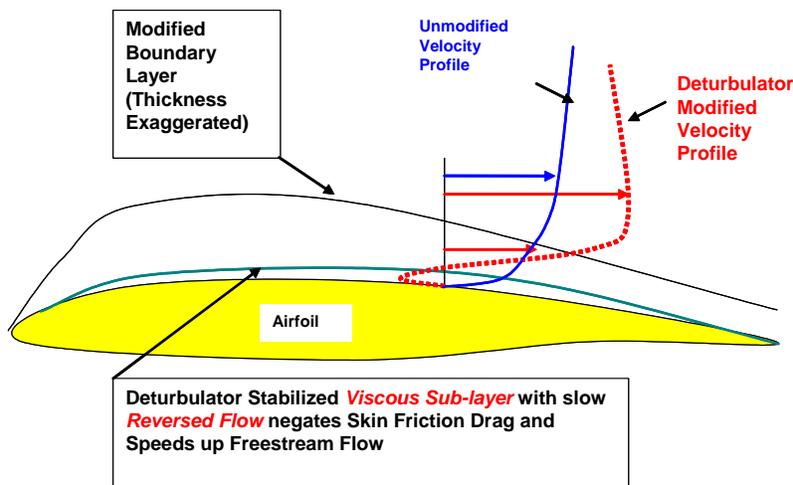

Modified Boundary Layer (Thickness Exaggerated)

Unmodified Velocity Profile

Deturbulator Modified Velocity Profile

Airfoil

Deturbulator Stabilized *Viscous Sub-layer* with slow *Reversed Flow* negates Skin Friction Drag and Speeds up Freestream Flow

Fig 15. Sketch showing how FCSD reduces drag by maintaining thin stable separated regions.

VI.   Acknowledgements

VII.   References

[1]McGhee, R.J., Viken, J.K., Pfenninger, W., and Beasley, W.D., "Experimental Results for a Flapped NLF Airfoil with high L/D Ratio," NASA TM-85788, May 1984.

[2]Sinha, S.K., "System and Method for Using a Flexible Composite Surface for Pressure-Drop Free Heat Transfer Enhancement and Flow Drag Reduction," U.S. Patent Application filed Jan 31, 2003, PCT Intl Patent Application filed Feb 3, 2003, (USPTO Publication No. US-2003-0145980-A1, Aug 2003a).

[3]Bushnell, D.M. and Hefner, J.M., "Effect of Compliant Wall on Turbulent Boundary Layers," *Physics of Fluids,* Vol. 20, No. 10., Pt II, Oct 1977, pp. s31-s48.

[4]Carpenter, P.W., Lucey, A.D. and Davies, C., "Progress on the Use of Compliant Walls for Laminar Flow Control," *J. of Aircraft*, Vol.38, No.3, 2001, pp. 504-512.

[5]Sinha, S.K., and S.Ravande, "Sailplane performance improvement using a Flexible Composite Surface Deturbulaotor", (AIAA paper 2006-0447), January 2006.

[6]Liebeck, R.H., *J. of Aircraft*, Oct, 1973.

[7]Sinha, S.K., "System for Efficient Control of Separation using a Driven Flexible Wall," U.S. Patent No. 5,961,080, awarded October 5, 1999.

[8]Sinha, S.K., and Wang, H., AIAA Paper 99-0923, 1999.

[9]Washburn, A.E., Althoff Gorton, S., and Anders, S.G., "Snapshot of Active Flow Control Research at NASA Langley," (AIAA paper 2002-3155), June 2002.

[10]Sinha, S.K., and Zou, J., "On Controlling Flows with Micro-Vibratory Wall Motion," AIAA paper AIAA-2000-4413, August 2000.

[11] Sinha, S.K.,., "Flow Separation Control with Microflexural Wall Vibrations," *Journal of Aircraft*, Vol.38, No.3., May-June-2001, pp. 496-503.

[12] Mangla, N.L., "Controlling Dynamic Stall with an Electrically Actuated Flexible Wall," Ph.D. Dissertation, Mech Eng Dept, University of Mississippi, December 2002.

[13] Ravande**,** S.V., "Performance Improvement and Drag Reduction of Aircraft by Boundary Layer Control using a Flexible Composite Surface Deturbulator," M.S. Thesis, Mechanical Engineering Department, University of Mississippi, August 2005.

[14] Drela, M., 1996: XFOIL-Code for 2-D Airfoil Flow Computations, Mass Inst. Of Tech, Cambridge, MA

[15]Sinha, S.K. and Sinha, S., "Reducing Road Vehicle Air Resistance with a Deturbulator", AIAA Aerospace Sciences Meeting, 2007 (to be submitted).